CONSEQUENCES ON BUOYANCY LOSS IN CASE OF SUBSEA GAS DISPERSION

Alessio Pierro, Katia Cassano, Paolo Farinelli, Raffaella Perini, Francesco Ferrini,
TECHFEM SpA – Human and Sustainable Engineering

This paper was presented at the 15th OMC Med Energy Conference and Exhibition in Ravenna, Italy, September 28-30, 2021. It was selected for presentation by OMC 2021 Programme Committee following review of information contained in the abstract submitted by the author(s). The Paper as presented at OMC 2021 has not been reviewed by the Programme Committee.

ABSTRACT

Hydrocarbon releases are events originated from **pipeline leaks ruptures**, that could occur for accidental events during operating life, maintenance phase or in case of **subsea tie-in installation**.

Subsea release is one of the main events to be accounted for **offshore risk assessment**. The accidents caused by **pipeline hydrocarbons leak** lead to explosions, fire and buoyancy loss.

When a subsea pipeline is ruptured, the pressurized gas rise at sea surface in bubbles form. Due to significant drag forces, the bubbles break and the plume will begin to disperse in atmosphere.

The **buoyant bubble plume** rises to the surface, spreading radially and entrains water, introducing a recirculation. The gas presence changes the local density, mainly at sea surface where this variation could induce a **buoyancy loss**, important aspect for ships and other floating structures. Several approaches can be used to analyze the problem.

Empirical and integral models provide a good representation of the phenomena but they are based on simplifications, moreover they are not able to model the sea surface behavior, crucial since is the zone where interactions with offshore structures, vessels and floating installations occur.

In this work a **Computational Fluid Dynamic** approach is proposed, carried out with the freeware software **OpenFOAM**, simulating the multiphase system with dispersed gas, seawater and air, in order to study in detail the subsea **gas bubbles cone** and the surface interactions, with the aim of analyze the possible consequences in terms of buoyancy loss.

The adoption of **CFD approach** gives to the safety engineer a powerful tool to investigate the problem, also including the environmental effects like wind and **sea currents**.

INTRODUCTION

Hydrocarbon releases are events originated from pipeline leaks ruptures. In particular, subsea release events are part of accidental scenarios included in the risk assessment of offshore installations. The accidents caused by pipeline hydrocarbons leak are countless and a considerable number of these leaks lead to explosions, fire or other hazardous scenario as loss of buoyancy [1]. In case of break of a subsea pipeline, the pressurized gas rises up to the sea surface in in form of bubbles. Due to the significant drag forces, the sea plume scatters in the atmosphere because of the bubbles break up. At the same time, the buoyant bubble plume rises to the sea surface by spreading radially, entraining water and inducing recirculation [2]. The plume behaviour depends on a number of factors, like release rate, release phase and environmental conditions [3].

From a mathematical point of view, the radial profiles of liquid velocity field, gas concentration and bubble frequency are usually approximated by Gaussian-like functions, to make the consequence assessment feasible. To do that, however, the quantitative impact of the gas release must be

evaluated precisely, possibly using an experimental approach. Nevertheless, such an approach is too expensive, dangerous and resource-consuming to be used systematically. Therefore, three methods are usually adopted to the scope:

- Empirical models
- Integral models
- Computational Fluid Dynamic (CFD) models

Empirical and integral models provide a good representation of the phenomena but they are based on quite unrealistic simplifications, like the absence of sea currents. Moreover, both of them cannot take into account the interactions with offshore structures, vessels and floating installations, because they are not able to model the see surface behaviour. On the contrary, CFD-based approaches are able to describe with a greater level of detail the behaviour of the three-phase system, providing additional information about bubble plume and sea surface one [4].

In this context, the present study focuses on the modelling and simulation of submerged gas dispersion from offshore pipelines using a CFD approach, aiming at eventually analysing and preventing possible damages to offshore structures causing potential severe limitations to the ships traffic.

DESCRIPTION OF THE SYSTEM

The analysed phenomena are the release of natural gas from a realistic subsea pipeline with external diameter of 36" (0.9144 m).

The sealine in analysis connects an offshore platform with an onshore processing plant, for a total length of 89 km. The sealine position are marked with the so-called “Kilometre Point” (KP), where KP = 0 km corresponds to onshore process plant and KP = 89 km to offshore platform. The values of water depth considered in this work are 15 m and 55 m, which are the extreme values along the route of pipeline (Fig 1: Sealine BathymetryFig 1) [2]. Below a water depth of 15 m the pipeline is trenched.

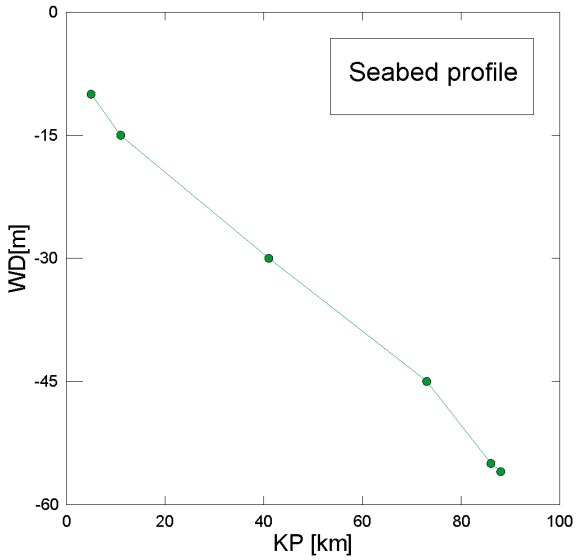

Fig 1: Sealine Bathymetry

Furthermore, dealing with pipelines it is necessary to consider the profiles of pressure and temperature inside the pipeline along the route. The operating conditions considered in the present analysis are reported in Fig 2. In the particular case-study considered, a water depth of 15 m is measured approximatively at KP =11 km with a corresponding pressure of 117 barg and

temperature of 30°C in the pipe, whereas a water depth of 55 m is measured approximatively at KP = 86 km with a corresponding pressure of 137 barg and temperature of 85°C in the pipe.

Two discharge flow rates of gas are considered for each depth: a) 1.5% of the design flow rate and b) the Full-Bore flow rate, which corresponds to the whole design flow rate (100%), equal to 1310 MMSCFD (1.46 106 Nm3/h). These two percentage values of release flow rate are selected as representative of two opposite situations: small damage (1.5%) and total rupture one (100%).

Since the gas release behaviour is influenced by the environmental conditions, values for wind velocity and sea current are set for simulation. As for the former, two Pasquill stability classes are considered: the class F2 (i.e., a wind velocity of 2 m/s) and the class D10 (i.e., a wind velocity of 10 m/s). As for the sea current, a velocity of 1.08 m/s is set at the sea surface. The air humidity is not considered in this study because it is not influential in the gas release behaviour.

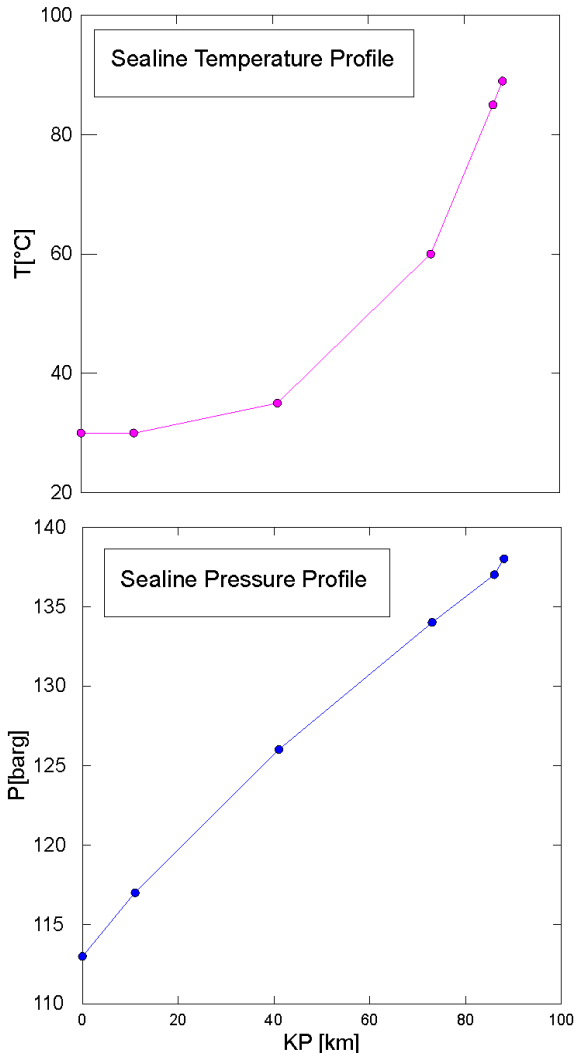

Fig 2: Pressure and Temperature Profile along the route.

COMPUTATIONAL METHODOLOGY

This section reports the details of the computational methodology used in the simulations. To this regard, we consider here 2D geometries for our systems to minimise the computational cost with the aim at obtaining the simulation results with the minimum computational cost but anyway enough degree of complexity to proceed with a sufficiently detailed consequence analysis.

GEOMETRY DESCRIPTION

In particular, the computational domain is composed of two different fluid sections: the air over the sea surface and the seawater. The effect of the wind is considered in the former, whereas the influence of the current stream is included in the latter. The pipeline is not considered in the simulation, as the release velocity of the gas at the hole (rupture) is set as boundary condition and calculated analytically according to the expression reported in Eq. 4. Due to the high release velocity, we have considered a total x-length of the order of 800 m for our geometries, although we have changed this value from case to case to be able to observe the entire flow field profile in its significant extension. Anyway, the geometry size considered makes our simulation full-scale and representative of a real pipeline section environment.
Furthermore, the geometry size is also chosen in order to avoid boundary effects, which can falsify the obtained results.
Another parameter changing from case to case is the hole size of the rupture, as the percentages of the maximum release flow rate considered that depend on the differential pressure (variable) between inside and outside the pipe and, thus, on the specific value of release velocity. The hole size used in each simulation is reported in Table 1.

Tab. 1: Pipeline Rupture scenarios considered in this work

Gas Release Rate							
Small-breaks case (1.5%)				*Full-bore case (100%)*			
P_{in} [barg]	P_{ext} [barg]	P_{in} [barg]	P_{ext} [barg]	P_{in} [barg]	P_{ext} [barg]	P_{in} [barg]	P_{ext} [barg]
117	1.49	137	5.49	117	1.49	137	5.49
D_{hole} [cm]		D_{hole} [cm]		D_{hole} [cm]		D_{hole} [cm]	
5.6		4.1		85		85	
Sea Current [m/s] = {0, 1.08}							

EVALUATION OF GAS RELEASE VELOCITY AT THE PIPE SURFACE

Fluid flow can be usually described as either an isothermal process or an adiabatic one. In our work, it is considered as an isentropic and adiabatic process.

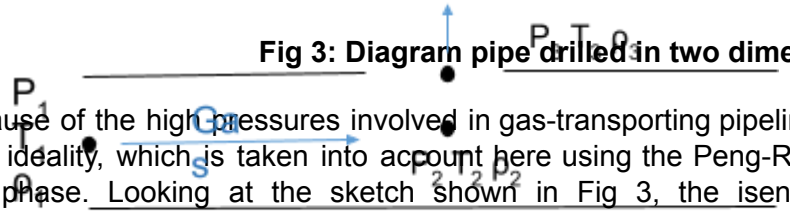

Fig 3: Diagram pipe drilled in two dimensions.

Because of the high pressures involved in gas-transporting pipeline, there is a significant deviation from ideality, which is taken into account here using the Peng-Robinson equation of state for the gas phase. Looking at the sketch shown in Fig 3, the isentropic expansion of gas occurs completely between point 2 – i.e., on the tube symmetry axis in correspondence of the centre of the hole – and point 3 – i.e., on the tube surface at the centre of the hole. Eq. 1 is used to calculate mass flow [5]:

$$Q = C_o A_{or} P_2 \sqrt{\frac{2Mw}{zRT_2}\frac{k}{k+1}\left[\left(\frac{P_3}{P_2}\right)^{\frac{2}{k}} - \left(\frac{P_3}{P_2}\right)^{\frac{k+1}{k}}\right]} Q = C_o A_{or} P_2 \sqrt{\frac{2Mw}{zRT_2}\frac{k}{k+1}\left[\left(\frac{P_3}{P_2}\right)^{\frac{2}{k}} - \left(\frac{P_3}{P_2}\right)^{\frac{k+1}{k}}\right]} \quad (1)$$

where Mw is the molecular weight in kg/mol, k the specific heats ratio (equal to 1.27 for natural gas), R the universal gas constant, A_{or} A_{or} the hole area and Co an empirical discharge coefficient, which is 0.61 for subsonic flow and Reynolds number higher than 30000, whereas is equal to the unity for other situations [5].
The value of the release speed at the orifice depends on whether the flow is sonic or subsonic. Since the sound speed in the seawater is within the range of 1460-1560 m/s, we consider a subsonic flow for the gas release, which is set as constant and equal to the initial release rate. Furthermore, in our system, the pressure P_2 P_2 is considered equal to P3, with both equal to the value of the hydrostatic pressure in that point of the sea. To obtain the velocity at the orifice, we start from writing the expression of the mass flow rate:

$$Q = A_{or}\rho_3 v_3 \; Q = A_{or}\rho_3 v_3 \tag{2}$$

where ρ_3 ρ_3 is the density at the point 3, given by an isentropic expansion from point 2 to point 3 according to the following polytropic expression:

$$\frac{P_3}{P_2} = \left(\frac{\rho_3}{\rho_2}\right)^{\frac{2}{k}} \frac{P_3}{P_2} = \left(\frac{\rho_3}{\rho_2}\right)^{\frac{2}{k}} \tag{3}$$

Obtaining ρ_3 from Eq. 3 and combining Eq. 2 with Eq. 1, we finally achieve an explicit expression for the release velocity v_3 v_3 (Eq. 4):

$$v_3 = \frac{C_o P_2}{\rho_3}\sqrt{\frac{2Mw}{zRT_2}\frac{k}{k+1}\left[\left(\frac{P_3}{P_2}\right)^{\frac{2}{k}} - \left(\frac{P_3}{P_2}\right)^{\frac{k+1}{k}}\right]} \; v_3 = \frac{C_o P_2}{\rho_3}\sqrt{\frac{2Mw}{zRT_2}\frac{k}{k+1}\left[\left(\frac{P_3}{P_2}\right)^{\frac{2}{k}} - \left(\frac{P_3}{P_2}\right)^{\frac{k+1}{k}}\right]}$$

(4)

NUMERICAL APPROACH

The hybrid method is applied above all on dispersed flows and complex multiphase flows. This method consists in coupling multiphase fluid model and VOF model, which is made possible thanks to the correspondence between the indicator function for tracking the interface in the VOF model and the volume fraction variable present in the Euler-Euler approach[6]. In practice, this is done to avoid the major disadvantages of one approach by exploiting the advantage of the other one. In particular, the major limitation of the VOF model, consisting in the shared momentum formulation, is overcome by the introduction of the multiphase Euler approach. On the other hand, the major limitation of the multiphase Euler approach, which does not explicitly track the interface, it is overcome by the introduction of the VOF method. In addition, the coupling of two approaches prevents numerical diffusion at the interface [7]. In OpenFOAM®, the hybrid method is developed through the combination of Euler-Euler multi-fluid method and sharp interface capturing (VOF). They named it as MultiphaseeulerFoam, whose characteristic equations are listed below. For incompressible, isothermal flows, mass and momentum equations for each phase k are [8]:

- *Continuity Equation*

$$\frac{\partial \alpha_k}{\partial t} + \overrightarrow{u_k} \cdot \nabla \alpha_k = 0 \frac{\partial \alpha_k}{\partial t} + \overrightarrow{u_k} \cdot \nabla \alpha_k = 0 \quad (5)$$

- *Momentum Equation*

$$\frac{\partial}{\partial t}(\alpha_k \rho_k \overrightarrow{u_k}) + (\alpha_k \rho_k \overrightarrow{u_k} \cdot \nabla)\overrightarrow{u_k} = -\alpha_k \nabla \mathrm{p} + \nabla \cdot (\alpha_k \rho_k \nabla \overrightarrow{u_k}) + \alpha_k \rho_k g + M_k$$

$$\frac{\partial}{\partial t}(\alpha_k \rho_k \overrightarrow{u_k}) + (\alpha_k \rho_k \overrightarrow{u_k} \cdot \nabla)\overrightarrow{u_k} = -\alpha_k \nabla \mathrm{p} + \nabla \cdot (\alpha_k \rho_k \nabla \overrightarrow{u_k}) + \alpha_k \rho_k g + M_k \quad (6)$$

In this paper, the term $M_k\, M_k$ is composed by drag, lift, virtual mass, turbulent dispersion force and surface tension force $F_{st}\, F_{st}$. The following equation is used for interface sharpening method that makes it possible to give a sharp interface between phases.

$$\frac{\partial \alpha_k}{\partial t} + \overrightarrow{u_k} \cdot \nabla \alpha_k + \nabla \cdot [u_c \alpha_k (1 - \alpha_k)] = 0 \frac{\partial \alpha_k}{\partial t} + \overrightarrow{u_k} \cdot \nabla \alpha_k + \nabla \cdot [u_c \alpha_k (1 - \alpha_k)] = 0$$

(7)

$(1 - \alpha_k)\,(1 - \alpha_k)$ ensures the presence of this term only in the interface region. The averaged conservation equations are locally influenced by phase contained in a that region. This influence is executed by phase indicator function $I_k(x,t)\, I_k(x,t)$ defined as:

$$\begin{cases} 1 \; if \; considered \; point \; is \; in \; phase \; k \\ 0 \; otherwise \end{cases} \begin{cases} 1 \; if \; considered \; point \; is \; in \; phase \; k \\ 0 \; otherwise \end{cases}$$

(8)

The probability that the point (x,t) is in the phase k is calculated with phase volume fraction, ensemble average of $I_k(x,t)\, I_k(x,t)$ [6]:

$$\alpha_k = \overline{I_k(x,t)}\; \alpha_k = \overline{I_k(x,t)} \quad (9)$$

As for the modelling of turbulence, the k-ε model is used, which computes turbulent kinetic energy k and turbulence length scale (or equivalent). Generally, the turbulence model is applied to the continuous phase only, but in our simulations the equations for turbulence are solved for all phases. The details of the turbulence equations are reported as follows in terms of kinetic energy k and turbulence energy dissipation rate ε:

$$\frac{\partial}{\partial t}\left((1-\alpha)\rho_c k_c\right) + \frac{\partial}{\partial x_j}\left((1-\alpha)\rho_c U_{i,c} k_c\right) = (1-\alpha)\left(S_k - \left(P_{k,c} - \rho_c \varepsilon_c\right)\right)$$

$$\frac{\partial}{\partial t}\left((1-\alpha)\rho_c k_c\right) + \frac{\partial}{\partial x_j}\left((1-\alpha)\rho_c U_{i,c} k_c\right) = (1-\alpha)\left(S_k - \left(P_{k,c} - \rho_c \varepsilon_c\right)\right)_+$$

$$+ \frac{\partial}{\partial x_j}\left[(1-\alpha)(\mu_c + \frac{\mu_{T,c}}{\sigma_k})\frac{\partial k_c}{\partial x_j}\right] + \frac{\partial}{\partial x_j}\left[(1-\alpha)(\mu_c + \frac{\mu_{T,c}}{\sigma_k})\frac{\partial k_c}{\partial x_j}\right]$$

(10)

$$\frac{\partial}{\partial t}((1-\alpha)\rho_c\varepsilon_c)+\frac{\partial}{\partial x_j}\left((1-\alpha)\rho_c U_{i,c}\varepsilon_c\right)=(1-\alpha)S_\epsilon-(1-\alpha)\frac{\varepsilon_c}{k_c}\left(C_{\epsilon 1}P_{k,c-}C_{\epsilon 2}\rho_c\varepsilon_c\right)+$$

$$+\frac{\partial}{\partial x_j}\left[(1-\alpha)(\mu_c+\frac{\mu_{T,c}}{\sigma_\epsilon})\frac{\partial\varepsilon_c}{\partial x_j}\right]+\frac{\partial}{\partial x_j}\left[(1-\alpha)(\mu_c+\frac{\mu_{T,c}}{\sigma_\epsilon})\frac{\partial\varepsilon_c}{\partial x_j}\right]$$

(11)

where $P_{k,c}$ $P_{k,c}$ is the production term induced by shear, S_k S_k and S_ϵ S_ϵ are the source terms due to bubble-induced turbulence. For each phase, the eddy viscosity is estimated as:

$$\mu_{t,c}=C_\mu\rho_c\frac{{k_c}^2}{\varepsilon_c}\ \mu_{t,c}=C_\mu\rho_c\frac{{k_c}^2}{\varepsilon_c} \qquad (12)$$

Since the energy lost through the drag force of the bubbles is converted to turbulent kinetic energy, the turbulent kinetic energy source can be expressed as :

$$S_k=KF_d\mathrm{U}_r\ S_k=KF_d\mathrm{U}_r \qquad (13)$$

where, K is a coefficient to tune the turbulent source, F_d F_d is the drag force and U_r U_r the relative velocity. A different expression is developed for S_ϵ S_ϵ considering the time scale of bubble-induced turbulence τ τ:

$$S_\epsilon=\frac{C_\epsilon}{\tau}S_k\ S_\epsilon=\frac{C_\epsilon}{\tau}S_k \qquad (14)$$

For liquid phases, in addition to the k-ε model, a multiphase formulation for Reynolds stress-tensor is additionally used.

$$\frac{\partial}{\partial t}\left((1-\alpha)\rho_c R_{ij}\right)+\frac{\partial}{\partial x_j}\left((1-\alpha)\rho_c U_{i,c}R_{ij}\right)=(1-\alpha)\left(S_{ij}+P_{ij}+\Phi_{ij}-\varepsilon_{ij}\right)+\frac{\partial}{\partial x_j}\left[(1-\alpha)D_{ij}\right]$$

$$\frac{\partial}{\partial t}\left((1-\alpha)\rho_c R_{ij}\right)+\frac{\partial}{\partial x_j}\left((1-\alpha)\rho_c U_{i,c}R_{ij}\right)=(1-\alpha)\left(S_{ij}+P_{ij}+\Phi_{ij}-\varepsilon_{ij}\right)+\frac{\partial}{\partial x_j}\left[(1-\alpha)D_{ij}\right] \qquad (15)$$

$$R_{ij}=\frac{\tau_{ij}^{Re}}{\rho_c}\ R_{ij}=\frac{\tau_{ij}^{Re}}{\rho_c} \qquad (16)$$

where D_{ij} D_{ij} the Reynolds stress diffusion and Φ_{ij} Φ_{ij} is the pressure-strain model for pressure fluctuations [9].

COMPUTATIONAL MESH

To give an idea of the size selection for computational mesh, each case analyzed was first modelled in a “static mode” (i.e., in the absence of wind and sea currents), which gives an indication of the plume extension, suggesting at the same time the most convenient domain length for the complete analyses (i.e., considering wind and sea currents). Another parameter changing from case to case is the hole size of the rupture, as the percentage of the maximum release flow

rate and, thus, on the specific value of release velocity. Typical domain characteristic values are reported in Tab. 2. The larger mesh dimensions entail a mesh finer near the hole and sea surface, and coarser towards the domain limits, as shown in Fig 4.

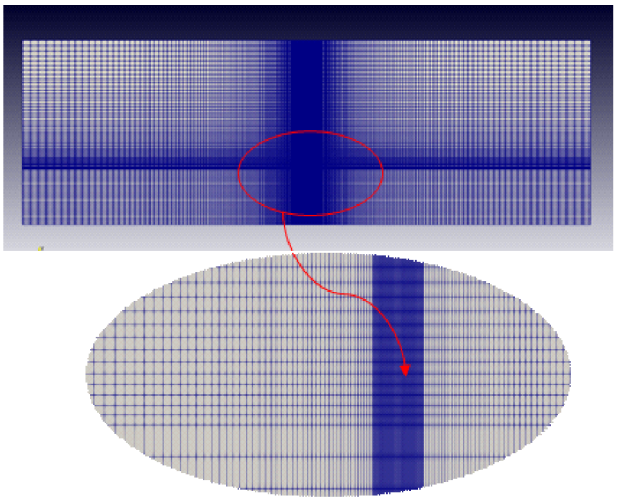

Fig 4: Example of computational mesh used for simulation. Static conditions, percentage discharge flow rates of 1.5% and water depth of 15m).

Tab. 2: Typical domain size

Case	*Nodes*	*Size*		*Minimum Element Size*		*Maximum Element Size*	
		X-length	Y-length	X-length	Y-length	X-length	Y-length
Water depth 15m, Release rate: 1.5%	92'092	400 m	50 m	0.0112 m	0.17 m	4 m	1.4 m
Water depth 15m, Release rate: 100%	148'512	650 m	50 m	0.057 m	0.17 m	4 m	1.5 m
Water depth 55m, Release rate: 1.5%	152'812	700 m	100 m	0.0112 m	0.17 m	5 m	1.4 m
Water depth 55m, Release rate: 100%	230'552	700 m	100 m	0.057 m	0.17 m	4 m	1.5 m

MODEL VALIDATION

The model has been validated against a series of lab scale experiment by Sridher et al. [10]. They performed a series of experiments with pipe of 2inch diameter, 12inches length and 1inch aperture with 3/4th inch brass gas inlet nozzle in a tank with dimensions 2mx1,5mx1,25m. Air is used as experimental gas. To validate the CFD model for subsea release, a simulation model having the same scale with the experimental pipe is built in OpenFoam. Air was released from the pipe at gas rates of 0.0112 m3/s with four different water depth values (0.5 m, 0.75 m, 1 m, 1.5 m). Plume diameter and centreline velocity profiles were measured and compared with CFD simulation results.

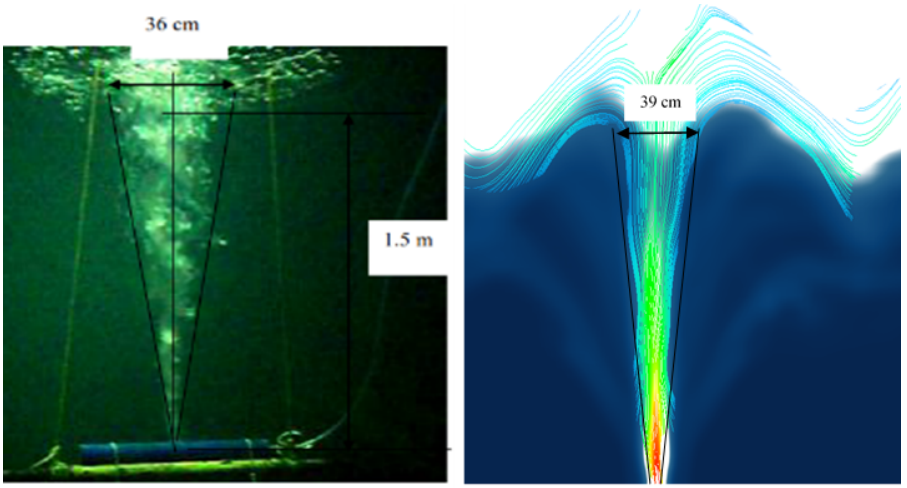

Fig 5: Plume behavior in experiment and in CFD simulation with 1,5 m of water depth and 0.0112 m3/s of gas flowrate.

In Fig 6 the comparison of experimental results and CFD results for the same flow rate at varying water depths are shown. Overall, the simulations results are in good agreement with experiments, which is considered adequate for the validation of simulation model for estimating plume diameter, gas outlet velocity and plume extension at sea surface.

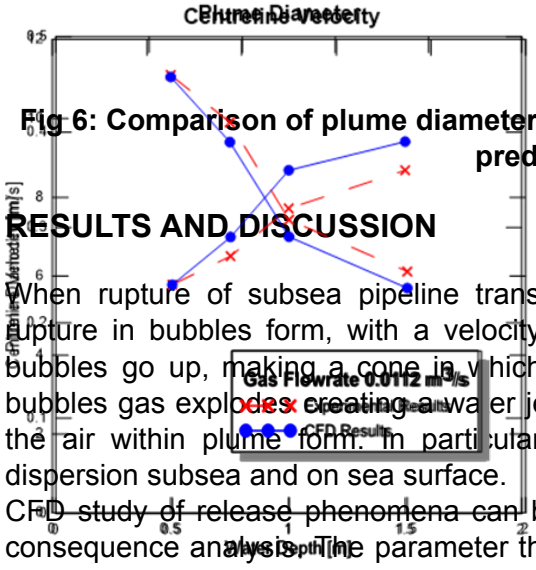

Fig 6: Comparison of plume diameter and centreline velocity observed in experiments and predicted by CFD model.

RESULTS AND DISCUSSION

When rupture of subsea pipeline transporting natural gas occurs, natural gas come out from rupture in bubbles form, with a velocity depending on hole rupture operating conditions. These bubbles go up, making a cone in which surrounding sea water is drag upward. At sea surface, bubbles gas explodes creating a water jet of variable height. Consequently, gas cloud disperses in the air within plume form. In particular has investigated sea density change, for gas bubble dispersion subsea and on sea surface.

CFD study of release phenomena can be useful in safety field. In detail, results can be used for consequence analysis. The parameter that has to be analysed in this study is sea density variation for subsea dispersion scenario, in order to verify the local buoyancy in case of release. This approach indicates what areas are dangerous for offshore structure, vessels and people eventually present.

Tab. 3: summary table of the study cases

	CASE 1	CASE 2	CASE 3	CASE 4	CASE 5	CASE 6	CASE 7	CASE 8
Water Depth [m]	15	15	15	15	55	55	55	55
%Release Rate	1,5	1,5	100	100	1,5	1,5	100	100
Wind Velocity [m/s]	2	10	2	10	2	10	2	10

EFFECT OF THE SEA CURRENTS

As mentioned before, seawater movements are influenced by sea currents. Bubble cone is inclined in direction of sea currents and inclination angle is function of different variables. Green line in each graph represent simulation in static conditions, orange and blue line represent results at wind velocity 2 and 10 m/s.

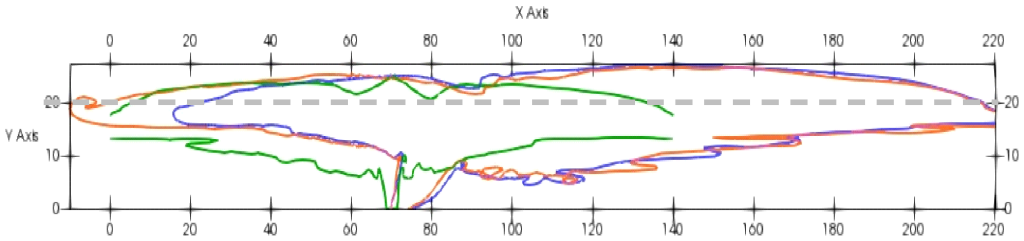

Fig 7: Mean volumetric phase fraction contours of static case, Case 1 and Case 2

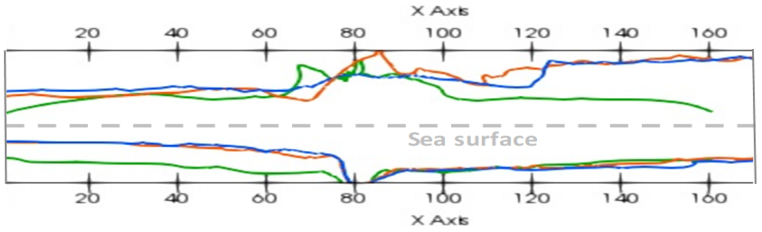

Fig 8: Mean volumetric phase fraction contours of static case, Case 3 and Case 4

Observing Fig 7 and Fig 8, it can be affirmed that a bigger flow rate implies a lower inclination angle, since gas flow is less influenced by sea current. In addition, since the sea currents increase the inclination of bubble cone, a greater gas dispersion in water occur, enlarging the diameter of cone at sea surface. In Fig 9 are illustrated results for 55m of water depth and 1,5 % of release rate. It is clear that greater water depth implies bigger bubbles cone at sea surface. Therefore, with the increase of water depth dimensions of bubbles cone grow.

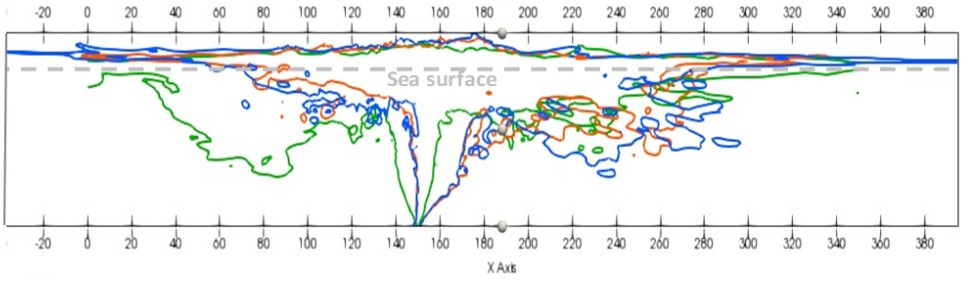

Fig 9: Mean volumetric phase fraction contours of static case, Case5 and Case 6

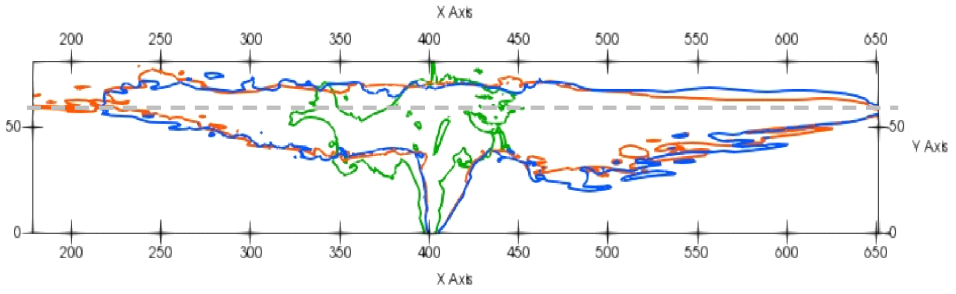

Fig 10: Mean volumetric phase fraction contours of static case, Case 7 and Case 8

Comparing Fig 9 and Fig 10, the observation that cone inclination angle decreases with the increase of release rate is confirmed.

EFFECT OF THE RELEASE RATE

In the following figures, gas behaviour is compared at the same water depth and wind velocity, varying the flow rate. A greater flow rate influences the plume size, both in air and in sea.

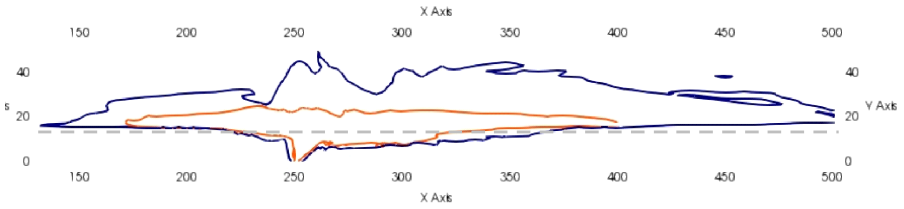

Fig 11: Mean volumetric phase fraction contours of Case 1 and Case 3

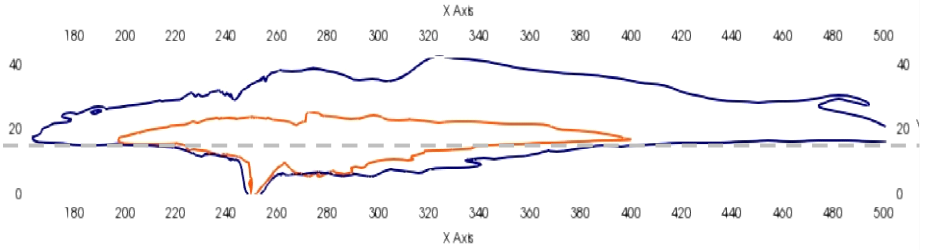

Fig 12: Mean volumetric phase fraction contours of Case 2 and Case 4

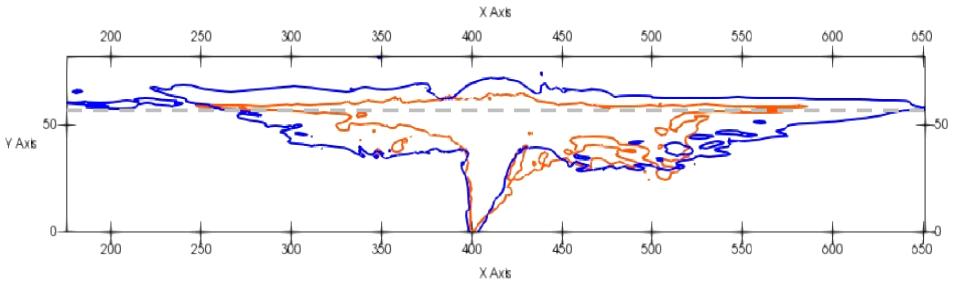

Fig 13: Mean volumetric phase fraction contours of Case5 and Case 7

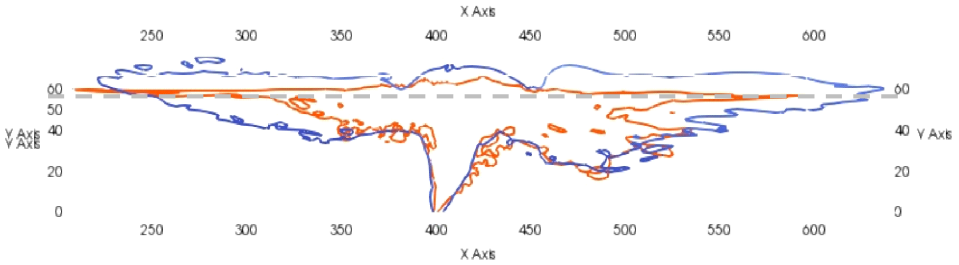

Fig 14: Mean volumetric phase fraction contours of Case 6 and Case 8

LOSS OF BUOYANCY

Buoyancy of ships or other floating objects depends on application of Archimedes principle. The buoyant force is defined as the vertical upward force generated by the fluid, acting on body. For Archimedes principle, buoyant force is proportional to weight of the fluid displaced. Mathematical definition of buoyant force is:

$$F_b = \rho g V \; F_b = \rho g V \tag{17}$$

Where ρ is fluid density, g is gravitational acceleration and V is volume of fluid displaced. Considering a floating body, two opposite forces in vertical direction act, that are weight force and buoyant force:

$$F_{tot} = g m_{sol} - \rho_{fluid} g V_{imm} = g(V\rho_{sol} - V_{imm}\rho_{fluid})$$

$$F_{tot} = g m_{sol} - \rho_{fluid} g V_{imm} = g(V\rho_{sol} - V_{imm}\rho_{fluid}) \tag{18}$$

$V_{imm}\, V_{imm}$ is the immersed volume of solid and V total volume of solid. The body floats when weight force and buoyant force are equal in module, and so when:

$$\frac{V}{V_{imm}} = \frac{\rho_{fluid}}{\rho_{sol}} \; \frac{V}{V_{imm}} = \frac{\rho_{fluid}}{\rho_{sol}} \tag{19}$$

If $\rho_{fluid1}\, \rho_{fluid1}$ is seawater density and $\rho_{fluid2}\, \rho_{fluid2}$ is the mean density between seawater and bubbles gas, therefore $\rho_{fluid1} > \rho_{fluid2}\; \rho_{fluid1} > \rho_{fluid2}$. This implies that buoyant force, where bubbles cone is present, will be lower and buoyancy should be checked, considering the fluid density reduction [11].

In following Figures are shown, for two cases, values of density at 80 s, when transitory effects are negligible. The density trend is irregular due to bubble presence.

In Fig 15 are reported the results of Case 1. Fig 15(a) shows the density distribution along the entire domain, while plot in Fig 15(b) shows the density values at sea surface, for each value of x. From this graph it is possible to identify the hazardous area for vessels, having a *diameter of about 150 m.* In Fig 16 are reported the results of Case 5. Fig 16 (a) shows the density distribution along the entire domain, while plot in Fig 16 (b) shows the density values at sea surface, for each value of x. From this graph it is possible to identify the hazardous area for vessels, having a diameter of about 180 m.

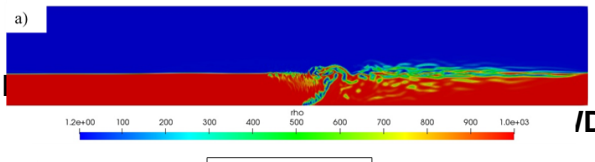

ı) and comparison between density values (b) on /D=15m, release rate=1,5% %, wind 2 m/s

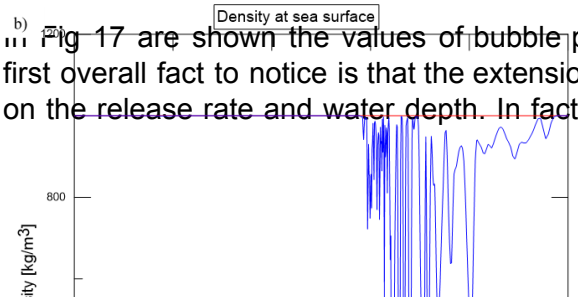

In Fig 17 are shown the values of bubble plume horizontal extension for each studied case. The first overall fact to notice is that the extension of the bubble plume at sea surface strongly depends on the release rate and water depth. In fact, at same water depth, for rupture with 100% flowrate,

the distance is much more than that with 1,5% flowrate. In this study, results at 55m of water depth show the bubble plume horizontal extensions larger than that at 15 m. This behaviour is related at bubble dispersion in seawater, that under the same flowrate, increases with water depth values.
Naturally, as show in Fig 17, wind velocity has not effect on extension of bubble plume, because this phenomenon develops only under seawater. Hazardous area with water depth 55m is greater than area at 15 m. This is caused by higher depth that imply more subsea dispersion. Another parameter that influence the section with density change is the release rate. In fact, a bigger release flowrate entails a bigger hazardous area. So, higher value of flowrate implies many bubbles and larger bubble plume diameter. Therefore, when a catastrophic rupture occurs on subsea pipelines, hazardous zone is much larger than that with smaller bore size.
Evaluate variations in seawater density induced by gas release simulations allows to identify gas bubble plume and his dimensions. Therefore, this output is useful to analyze an hazardous area connected to gas bubbles presence. In addition, if the sinking of the ship is related to momentum of rising bubbles and not at density seawater variations this study is still valid, since the numerical approach allows to evaluate the kinetic of the release.

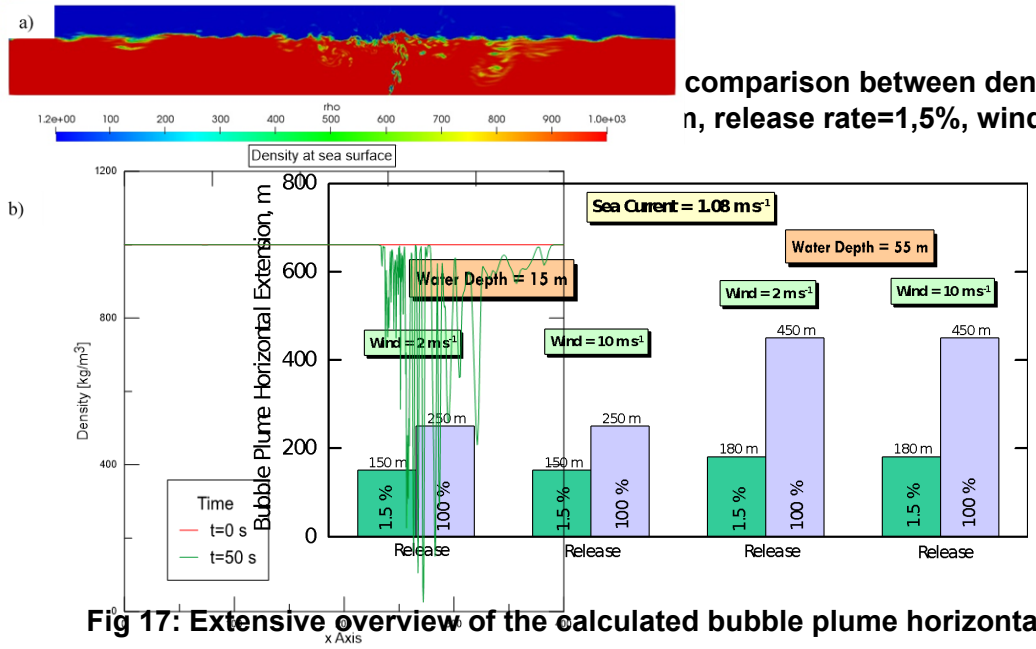

comparison between density values (b) on n, release rate=1,5%, wind 2 m/s

Fig 17: Extensive overview of the calculated bubble plume horizontal extension

All results are presented as two-dimensional areas because study is based on two-dimensional geometry. However, for real application, it could considerer a hazardous area with diameter equal to extension at sea surface with seawater density variation.

CONCLUSIONS

In this work, the subsea gas release phenomenon was studied by CFD simulations carried out by the open-source software OpenFoam in different conditions. The obtained results are useful for consequences analysis to consider hazard scenarios of buoyancy loss.

Underwater, gas rises up to the sea surface forming a cone-like shape, according to the literature, where some empirical models are used to reproduce the shape. However, both Empirical and Integral models, although providing a good representation for the cone behaviour, do not consider the gas plume at all. Therefore, the CFD approach is the only one allowing a better description of the fluid dynamic behaviour of both bubble plume and gas plume on the sea surface. For this purpose, multi-phase simulations were carried out to study the system in conditions close to the real ones, considering a 2D geometry instead of a 3D one to reduce the computational duty and

the run time. Nevertheless, this simplification did not affect the precision needed for the consequences analysis in risk scenarios.

Underwater, it was shown that gas rises the sea surface forming a cone-like shape up to a certain distance beneath the sea surface according to the literature. It was also found that, at 55 m depth, the cone diameter at the sea level is larger than that at 15 m due to dispersion of gas in the sea. On the contrary, different wind velocity values is observed not to change significantly the cone diameter. However, a value of 10 m/s of wind velocity makes plume shorter and higher with respect to the case with 2 m/s, due to the wind action against sea surface gas extension.

The bulk density variation of seawater is an important issue for QRA study of offshore activities and methodology shown in this study is useful to quantify sink scenario. Change in density value is not the only potential cause of vessels sink. In fact, small vessels or floating objects could be damaged by effect of upward drag due to motion at sea surface of the liquid entrained by the rising bubbles . This force would affect vessel stability. For large and heavy vessels, loss of buoyancy could have most serious consequences. When floating equipment are considered, the aspects to analyze are different and more complex, as for example the dynamic response of offshore structure. Anyway, CFD simulations is able to estimate consequences in terms of hazardous distances related to bubbles presence, regardless if there is a loss of buoyancy for change in bulk density or momentum product by rising bubbles.

This work represents only a first step in modelling and comprehension of sinking causes due to subsea gas release.

REFERENCES

[1] Lees, F. P., "*Loss Prevention in the Process Industries*", Reed educational and Professional Publishing, 1996, Volume 1,second edition.

[2] Smith, B.L., "On the modelling of bubble plumes in a liquid pool", *Applied Mathematical Modelling*, 1998.

[3] Rew, PJ, "Dispersion of subsea releases", *Rewiew of prediction Methodologies*, 1995.

[4] Cloete, S., "CFD modeling of plume and free surface behavior resulting from a sub-sea gas release", *Applied Ocean Research,* 2009.

[5] Yuhua, D., "Evaluation of gas release rate through holes in pipelines", *Journal of Loss Prevention in the Process Industries,* 2002.

[6] Tocci, F., *"Assessment of a hybrid VOF two-fluid CFD solver for simulation of gas-liquid flows in vertical pipelines in OpenFOAM®"*, Tesi di Laurea Magistrale in Ingegneria Aeronautica, Politecnico di Milano, 2016.

[7] Parsi M., "Assessment of a hybrid CFD model for simulation of complex vertical upward gas–liquid churn flow", *chemical engineering research and design*, 2016.

[8] Wardle, K.E., "Hybrid Multiphase CFD Solver for Coupled Dispersed/Segregated Flows in Liquid-Liquid Extraction", *chemical engineering research and design*, 2012.

[9] Colombo, M., "Multiphase turbulence in bubbly flows: RANS simulations*", International Journal of Multiphase Flow,* 2015.

[10] Sridher, P.C., "*Validating Sub-sea Gas Pipeline Leaks Discharge Model For Arabian Sea Conditions*", University Of Petroleum & Energy Studies, Dehradun, 2013.

[11] Wilson, K.J., "*The effects of gas aerated seas upon the buoyancy and stability of floating drilling vessels*", a thesis in petroleum engineering , at Texas Tech University,1987.